Journal of ELECTRONIC MATERIALS, Vol. 48, No. 4, 2019
https://doi.org/10.1007/s11664-019-06965-6

Role of Hydrogen Flow Rate on Microstructure of a-Si:H(n) Films: Spectroscopic Ellipsometry Studies

VENKANNA KANNEBOINA[1] and PRATIMA AGARWAL[1,2,3]

1.—Department of Physics, Indian Institute of Technology, Guwahati, Assam 781039, India.
2.—Centre for Energy, Indian Institute of Technology, Guwahati, Assam 781039, India.
3.—e-mail: pratima@iitg.ac.in

The influence of hydrogen flow rate on the microstructure and optical properties of phosphorous doped hydrogenated amorphous silicon (a-Si:H(n)) films is studied through spectroscopic ellipsometry (SE). A series of a-Si:H(n) films were deposited using radio frequency plasma enhanced chemical vapour deposition (RFPECVD) technique by varying the hydrogen flow rate (HFR) in the range of 30–80 SCCM. The SE measurements showed a shift in peak position of pseudo dielectric function of these films from 3.6 eV (for pure a-Si:H) to 4.1 eV with a shoulder peak at 3.4 eV (nanocrystallites embedded a-Si:H) as the hydrogen flow rate was increased. A systematic increase in crystalline fraction along with a decrease in void fraction was observed as HFR was increased up to 70 SCCM during deposition. The results confirm that hydrogen dilution helps in improving the microstructure of films and favours the formation of strong Si–H bonds. Beyond 70 SCCM of HFR, a large flux of hydrogen resulted in an increase in void fraction and disorder in the films.

Key words: a-Si:H(n) thin films, hydrogen flow rate, microstructure, spectroscopic ellipsometry

INTRODUCTION

Hydrogenated amorphous silicon (a-Si:H) films as solar cells have been extensively studied in the past.[1–7] However, market share of a-Si:H based solar cells could not be increased due to their relatively low efficiency and poor stability as compared to other technologies. The interest in amorphous silicon films is revived once again after Sanyo announced that c-Si/a-Si:H based heterojunctions with intrinsic thin layer (HIT) solar cells have comparable efficiency as those of conventional c-Si solar cells.[8–11] In these silicon heterojunction (SHJ) solar cells, doped a-Si:H film is used to fabricate the *p–n* junction on a c-Si wafer, whereas a thin intrinsic a-Si:H layer is used to passivate the interface defect states. The microstructure and the bandgap of both doped and intrinsic a-Si:H layers play a crucial role in the efficiency of these solar cells. However, neither epitaxial films nor films with large void fraction are good for the SHJ solar cells.[12,13] Many groups have demonstrated the importance of hydrogen in the formation of a-Si:H and nc-Si:H/μc-Si:H networks.[2,14–18] Adding hydrogen to silane during deposition results in the most stable and less defective a-Si:H films for solar cells.

Spectroscopic ellipsometry (SE) is a powerful tool to determine the optical constants, band gap and thickness of thin as well as ultrathin films.[19] The technique can be used both *in situ* as well *ex situ* and provides information on the microstructure of individual layers in a multilayer structure. The technique has, however, not been used by many research groups to study the microstructure and optical constant of a-Si:H(n) films.[20–24]

In the present paper, we report the SE studies on a series of phosphorous doped a-Si:H(n) films, deposited by varying the hydrogen flow rate during

(Received October 12, 2018; accepted January 16, 2019; published online January 31, 2019)

deposition of films. The phosphorous doped films are chosen since the reported efficiency of c-Si(p)/a-Si:H(n) SHJ cells are still low as compared to those of c-Si(n)/a-Si:H(p).[25,26] Through these studies, the aim is to understand the microstructure of a-Si:H(n) films and optimize the deposition parameters for fabricating the SHJ solar cells with higher efficiency. The SE measurements have been used to determine the optical bandgap, thickness and surface roughness of the films and also to estimate the void, amorphous and crystalline volume fraction. The results obtained from UV–Vis–NIR and atomic force microscope (AFM) measurements are compared with SE results.

EXPERIMENTAL DETAILS

Phosphorous doped hydrogenated amorphous silicon, a-Si:H(n), thin films were deposited on Corning 1737 glass substrate at a hydrogen flow rate (HFR) of 30–80 SCCM using RFPECVD in a multichamber (Excel Instruments) system with PH_3 (1% of PH_3 diluted in H_2) flow rate of 6 SCCM, pure silane flow rate of 4 SCCM, RF power of 30 W, process pressure of 0.42 mbar, and deposition temperature of 200°C. The HFR of 30–80 SCCM correspond to *MN87–MN92* films, respectively.

The a-Si:H(n) thin films deposited on Corning 1737 glass were characterised by *ex situ* SE (Sopra, GES5) technique in the photon energy range of 2–5.5 eV and at an incident angle of 70°. SEA software is used for analysis of the data of films.[27,28]

The thickness and bandgap of a-Si:H(n) films were estimated by the Tauc–Lorentz (TL) model.[29] In TL models, the expression for the imaginary part of the pseudo dielectric function of films is given by

$$\varepsilon_{2,\mathrm{TL}}(E) = \begin{cases} \left[\frac{AE_0C(E-E_g)^2}{\left((E^2-E_0^2)^2+C^2E^2\right)}\frac{1}{E}\right] & \text{for } E > E_g \\ 0 & \text{for } E \le E_g \end{cases} \quad (1)$$

where A is oscillator strength, E_0 is peak transition energy, E_g is optical band gap and C is broadening parameter.

The real part of the pseudo dielectric function of the films in the TL model is given by[29]

$$\varepsilon_{1,\mathrm{TL}}(E) = \varepsilon_1(\infty) + \frac{2}{\pi}P\int_{E_g}^{\infty}\frac{\xi\varepsilon_2(\xi)}{\xi^2-E^2}\mathrm{d}\xi, \quad (2)$$

where P represents the Cauchy principal part of the integral and $\varepsilon_1(\infty)$ is an additional fitting parameter.

The volume (void, amorphous and crystalline) fraction and surface roughness of the films was estimated by the Bruggeman Effective Medium Approximation (BEMA) model.[19,30,31] The expression of effective dielectric function $\varepsilon_{\mathrm{eff}}(E)$ of films is given by

$$\sum_i f_i \frac{\varepsilon_i(E)-\varepsilon_{\mathrm{eff}}(E)}{\varepsilon_i(E)+2\varepsilon_{\mathrm{eff}}(E)} = 0, \quad (3)$$

where $\varepsilon_i(E)$ is the dielectric function and f_i is the volume fraction of ith phase in composite material.

The UV–Vis–NIR spectrometer (Shimadzu 3101PC) was used to record the transmission spectra of the a-Si:H(n) thin films in the wavelength range of 200–2500 nm, and the optical band gap of the films was estimated from this spectrum. The surface morphology of a-Si:H(n) thin films was studied by AFM (Agilent 5500).

RESULTS AND DISCUSSION

Influence of Hydrogen Flow Rate on a-Si:H(n) Films

Figure 1a and b show the measured spectra of the real ($\langle\varepsilon_1\rangle$) and the imaginary ($\langle\varepsilon_2\rangle$) part of the pseudo dielectric function of a-Si:H(n) films and also c-Si as a function of photon energy. The intense peak in low energy range (around 2 eV) is due to interference of reflected light from the interface and surface of film and its position depends upon the thickness and refractive index of the films; the

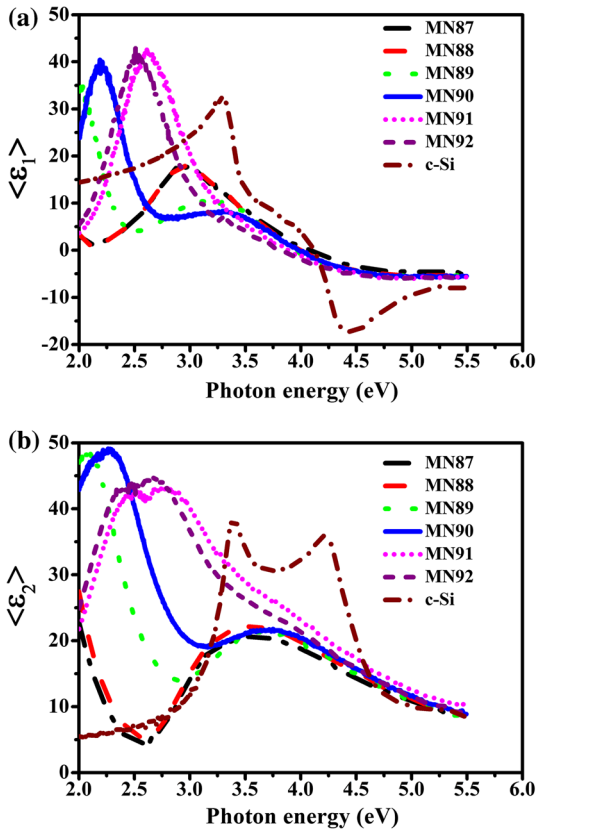

Fig. 1. (a) Real ($\langle\varepsilon_1\rangle$) and (b) imaginary ($\langle\varepsilon_2\rangle$) part of the pseudo dielectric function measured as a function of photon energy for a-Si:H(n) films along with c-Si substrate.

intensity of this peak also depends upon the substrate used. The peak position in $\langle\varepsilon_1\rangle$ and $\langle\varepsilon_2\rangle$ spectra has shifted from 2 eV to 2.5 eV with increase in HFR of a-Si:H(n) films. This indicates a change in thickness of the films with variation of HFR. In case of c-Si, the peak and dip in $\langle\varepsilon_1\rangle$ and two peaks in $\langle\varepsilon_2\rangle$ spectra at 3.4 eV and 4.2 eV correspond to direct band to band transition.[32] Similar features have also been reported for nc-Si:H, μc-Si:H films and crystalline silicon.[33,34]

The $\langle\varepsilon_2\rangle$ spectra of *MN87–MN89* (HFR of 30–50 SCCM) films show broad peak at 3.6 eV corresponding to direct band to band transitions in the a-Si:H films.[19,29,35] The peak has shifted to 3.7 eV for *MN90* (60 SCCM) film. For films deposited at HFR of 70 and 80 SCCM (*MN91* and *MN92*), the broad peak has further shifted to 3.9 eV and 4.1 eV with signature of a shoulder peak at 3.4 eV, respectively. This is an indication of change in microstructure of the films from pure amorphous phase to that near the onset of the nanocrystalline phase.[17,19,36–38] In case of *MN91* and *MN92,* the peak at 4.2 eV is integrated with a more dominating peak at 2.5 eV (interference fringe due to thickness of films). A systematic increase in the amplitude of $\langle\varepsilon_2\rangle$ spectra is also observed from *MN87–MN91* films, which has decreased for *MN92* film. The magnitude of $\langle\varepsilon_1\rangle$ and $\langle\varepsilon_2\rangle$ is highest for *MN91* film. The information about the film density, void fraction in films and also type of bonding configuration (Si–H, Si–H_2 and Si–H_n etc.) has been obtained from the amplitude of $\langle\varepsilon_2\rangle$ spectra.[35] A decrease in broadening accompanied by a higher amplitude in these $\langle\varepsilon_1\rangle$ and $\langle\varepsilon_2\rangle$ spectra suggest an improvement in density and decrease in disorder in the a-Si:H(n) films deposited at higher H_2 flow rate.

The Tauc–Lorentz (TL) model has been applied to calculate the thickness and optical bandgap of a-Si:H(n) films.[19,29,35] We have used the two-layer model structure (*substrate/bulk layer/surface roughness layer/air*) to determine the thickness, optical band gap and also volume fractions and surface roughness of a-Si:H(n) films as described elsewhere.[27,28] Figure 2a and b show the measured and fitted (TL model) values of the real ($\langle\varepsilon_1\rangle$) and the imaginary ($\langle\varepsilon_2\rangle$) part of the pseudo dielectric function of a-Si:H(n) films as a function of photon energy. Estimated thickness and optical band gap values are listed in Table I. The quality of fitting (goodness of fit) (R^2) is 99% and estimated errors are included in figures.

Figure 3 shows the TL model fitted parameters of a-Si:H(n) films as a function of hydrogen flow rate. Amplitude parameter (A) has increased and broadening parameter (C) has decreased with increase in the HFR of a-Si:H(n) film, except for *MN92* film. The main reason for this change is that a large flux of atomic hydrogen has passivated co-ordination defects and decreased the band tail states in a-Si:H network. In a-Si:H, hydrogen is mostly incorporated at Si dangling bonds or vacancies. However,

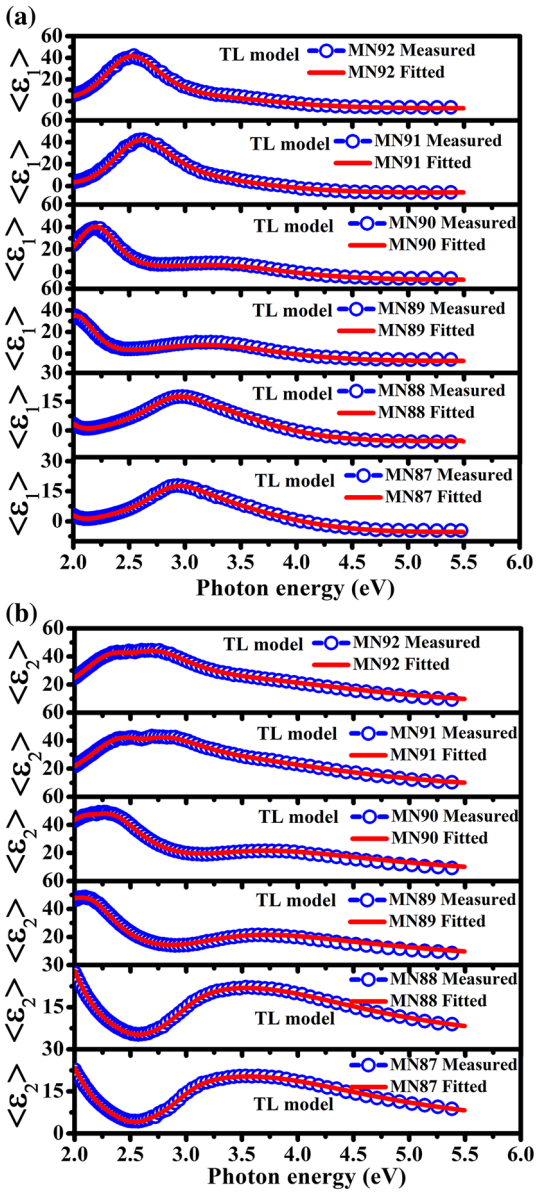

Fig. 2. (a, b) Measured and fitted (Tauc–Lorentz model) values of real ($\langle\varepsilon_1\rangle$) and imaginary ($\langle\varepsilon_2\rangle$) part of pseudo dielectric function of a-Si:H(n) films as a function of photon energy.

some hydrogen is also bonded as dihydrides which are expected to reside on the inner surface of the micro/nano voids. As the hydrogen flow rate is increased, more atomic hydrogen reaching the surface of the film could diffuse in the bulk of the film and break some Si–Si and Si–H_2 bonds replacing these with stronger Si–H bonds.[1] This improves the microstructure of the films. Further, during the growth of the films, some of these neighbouring Si–H bonds at the surface of voids may break and form H_2 molecules which leave the voids. The remaining free Si bonds then recombine forming the micro/nanocrystalline phase, thus increasing the crystallinity of the films.[39] For *MN92* (80 SCCM) film, the value of A has slightly decreased and C value has increased, which could be due to a very

Table I. The TL model fitted parameters (A, E_0, C and E_g) and estimated thickness of a-Si:H(n) films

Sample	HFR	Thickness (nm)	*A* (eV)	E_0 (eV)	*C* (eV)	E_g (eV)	d_s (nm)	E_g (eV) (UV–Vis–NIR)
MN87	30	109	225	3.50	2.87	1.80	1.76	1.81
MN88	40	98	225	3.54	2.78	1.81	1.82	1.82
MN89	50	75	227	3.61	2.75	1.84	1.33	1.83
MN90	60	67	232	3.70	2.67	1.85	1.50	1.85
MN91	70	62	247	3.94	2.55	1.86	1.35	1.87
MN92	80	53	245	4.11	2.80	1.86	1.54	1.87

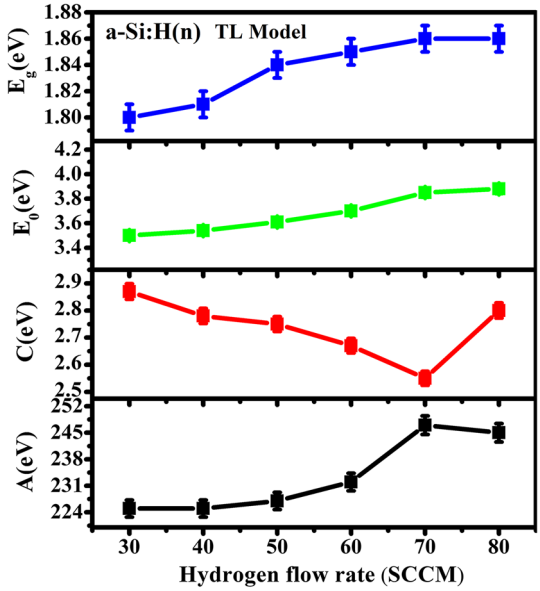

Fig. 3. The TL model fitted parameters (*A*, E_0, *C* and E_g) of a-Si:H(n) film as a function of hydrogen flow rate.

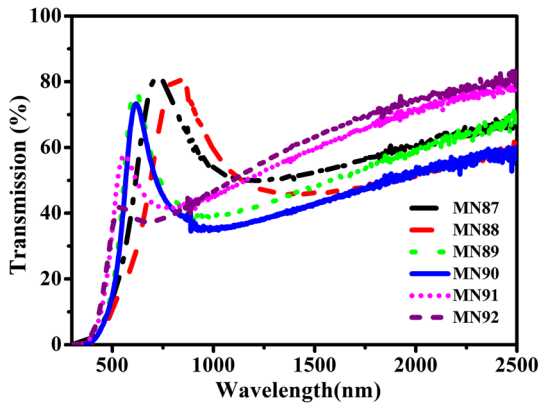

Fig. 4. The UV–Vis–NIR transmission spectra of a-Si:H(n) thin films.

high concentration of H radicals. At HFR of 80 SCCM, hydrogen concentration in the chamber is considerably high, thus hydrogen precursors make frequent collisions with neighbouring H_2 and SiH_4 precursors. As a result, some of growth precursors may not be able reach to the surface as well as the bulk of the films and also do not occupy stable positions on the growing surface. This leads to increase in defect density, bond density of Si–H_2 (formation of higher hydride) and void fraction in the films. Figure 4 shows the UV–Vis–NIR transmission spectra of *MN87–MN92* films. In Fig. 4, a clear shift in absorption edge of transmission spectra of films towards lower wavelength is observed with increase in HFR. The value of optical band gap of the films calculated using Tauc's plot[40] is listed in Table I. These values are in good agreement with those estimated from SE analysis. It is observed that thickness of the films has decreased and band gap has increased with increase in HFR during deposition. The trend is similar to that reported for undoped a-Si:H films.[27,41]

In order to estimate the amorphous, crystalline and void fraction in the films, the BEMA model was used.[19,27,28,30,31] Figure 5a and b show measured and fitted (BEMA model) spectra of the real ($\langle\varepsilon_1\rangle$) and the imaginary ($\langle\varepsilon_2\rangle$) part of the pseudo dielectric function of a-Si:H(n) films as a function of photon energy. Estimated volume fractions and surface roughness of films are given in Table II.

Figure 6 shows the void (f_v), amorphous (f_a) and crystalline (f_c) fractions of a-Si:H(n) films with respect to hydrogen flow rate. It is observed that void fraction has systematically decreased up to 70 SCCM of HFR and then increased at 80 SCCM of HFR. The least void fraction of 11.49% is observed at 70 SCCM of HFR (*MN91*), whereas the crystalline fraction has continuously increased. The maximum crystalline fraction of 13.49% is observed at 80 SCCM of HFR. The amorphous fraction is found to be nearly independent of HFR till 70 SCCM and then has decreased with further increase in HFR to 80 SCCM. The surface roughness of the films is found to increase from 1 nm to 3 nm with increase in HFR due to increase in grain size of the films.

Figure 7a, b, c, d, e and f show the AFM surface morphology of *MN87–MN92* thin films measured on a scan area of 2 × 2 μm^2 in non-contact mode. It is observed that all the films are uniform throughout the sample and formation of voids has taken place at lower HFR of the films. The RMS surface roughness (d_{RMS}) values are found to be 1.6 nm to 3.3 nm corresponding to *MN87* to *MN92* films respectively and also are listed in Table II. The grain size and roughness of the films has increased with increase in HFR of the films. The roughness of

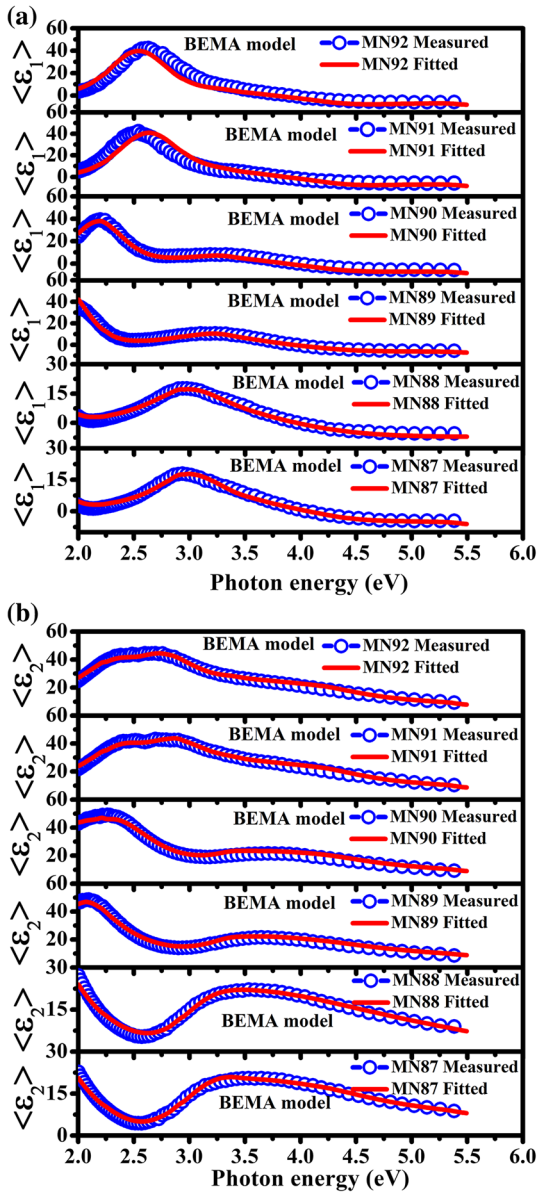

Fig. 5. (a, b) Measured and fitted (BEMA model) values of real ($\langle\varepsilon_1\rangle$) and imaginary ($\langle\varepsilon_2\rangle$) part of pseudo dielectric function of a-Si:H(n) films as a function of photon energy.

the films from the AFM studies is also quite similar to the estimated surface roughness of the films from SE measurements.

The films deposited at 30–50 SCCM of HFR are amorphous in nature and have a disordered Si network and most of the Si atoms are bonded as Si–H_2. SE analysis reveal that these films have low A, high C value and higher void fraction, as estimated by TL and BEMA models, respectively. The flux of atomic hydrogen in the plasma increases with increase in hydrogen flow rate. This hydrogen flux participates in many reactions during growth of the films with Si and H_2 precursors on the surface and as well as in bulk of the films. During deposition, the atomic hydrogen etches out some of the amorphous fraction and reconstructs the Si–Si and Si–H, Si–H_2 bonding configurations.[42] This results in structural transition from amorphous to nano/micro crystalline phase depending on hydrogen dilution of the precursor gases. The film microstructure, bonding arrangement, and Si–H bonding configuration are thus improved up to 70 SCCM of HFR of a-Si:H(n) films. Beyond these flow rates, rate of ion

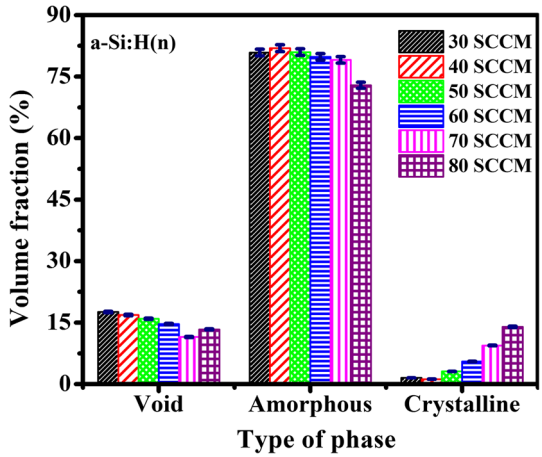

Fig. 6. The void, amorphous and crystalline volume fractions of a-Si:H(n) film corresponding to H_2 flow rate.

Table II. The estimated void, amorphous and crystalline volume fractions, thickness and surface roughness (d_s) of a-Si:H(n) films

Sample	HFR (SCCM)	Thickness (nm)	f_v (%)	f_a (%)	f_c (%)	d_s (nm)	d_{RMS} (nm) (AFM)
MN87	30	109	17.59	80.86	1.53	1.46	1.6
MN88	40	98	16.86	81.92	1.21	1.82	1.8
MN89	50	75	15.94	80.95	3.10	2.03	2.0
MN90	60	67	14.67	79.83	5.50	2.50	2.1
MN91	70	62	11.49	79.08	9.42	2.65	3.0
MN92	80	53	13.35	72.89	13.98	3.14	3.3

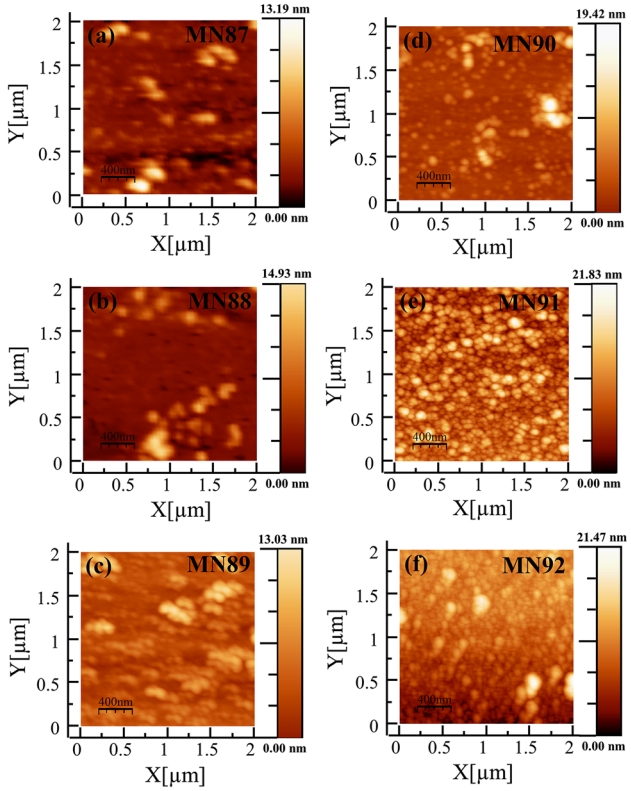

Fig. 7. (a–f) AFM surface morphology of *MN87–MN92* films.

bombardment has increased due to increased atomic hydrogen flux. This leads to formation of microvoids and the poor quality of the films at HFR of 80 SCCM. However, the crystalline fraction of the films has increased with increase in hydrogen flow rate of the films. Films deposited at higher HFR (60–80 SCCM) exhibit a change in microstructure from amorphous to near nanocrystalline nature.

CONCLUSION

Influence of hydrogen flow rate on microstructure, optical properties of a-Si:H(n) layer was studied by SE measurements. It is observed that microstructure of a-Si:H(n) films changes from amorphous to nanocrystalline phase by varying hydrogen dilution. This phase transition is confirmed by SE analysis; peak position and amplitude of $\langle \varepsilon_2 \rangle$ spectra has changed with variation of hydrogen dilution of films. The bandgap, surface roughness and crystallinity of the films has increased with increase in HFR of the films. It is found that less defective a-Si:H films with smaller void fraction and improved Si–H bond density are obtained at 70 SCCM of HFR of films. This optimised, improved microstructure and near onset of nanocrystalline phase of a-Si:H(n) films are very useful for fabrication and improve the performance of c-Si/a-Si:H solar cells.

ACKNOWLEDGMENTS

Financial support for fabricating the multichamber PECVD system was received from Department of Science and Technology (DST) (Grant No. DST/TM/SERI/2K11/78(G)), India and Defence Research and Development Organization (DRDO) (Grant No. ERIP/ER/0900376/M/01/1297), India. We acknowledge the Central instrument facility (CIF), IIT Guwahati for SE and AFM measurements.

REFERENCES

1 R.A. Street, *Hydrogenated Amorphous Silicon* (Cambridge: Cambridge University Press, 1991).
2. A. Matsuda, *J. Non Cryst. Solids* 338–340, 1 (2004).
3. H. Tanimoto, H. Arai, H. Mizubayashi, M. Yamanaka, and I. Sakata, *J. Appl. Phys.* 115, 073503 (2014).
4. R. Rao, F. Kail, and P.R. i Cabarrocas, *J. Mater. Sci. Mater. Electron.* 18, 1051 (2007).
5. P. Gogoi and P. Agarwal, *Sol. Energy Mater. Sol. Cells* 93, 199 (2009).
6. L. Hamui, B.M. Monroy, K.H. Kimb, A. López-Suárez, J. Santoyo-Salazar, M. López-López, P.R. i Cabarrocas, and G. Santana, *Mater. Sci. Semicond. Process.* 41, 390 (2016).
7. A.R. Zanatta and I. Chambouleyron, *Phys. Rev. B* 53, 3833 (1996).
8. Y. Tsunomura, Y. Yoshimine, M. Taguchi, T. Baba, T. Kinoshita, H. Kanno, H. Sakata, E. Maruyama, and M. Tanaka, *Sol. Energy Mater. Sol. Cells* 93, 670 (2009).
9. M. Taguchi, A. Yano, S. Tohoda, K. Matsuyama, Y. Nakamura, T. Nishiwaki, K. Fujita, and E. Maruyama, *IEEE J. Photovolt.* 4, 96 (2014).
10. M.A. Green, Y. Hishikawa, A.W.Y.H. Baillie, E.D. Dunlop, and D.H. Levi, *Prog. Photovolt. Res. Appl.* 26, 3 (2018).
11. J. Zhao, A. Wang, and M.A. Green, *Sol. Energy Mater. Sol. Cells* 65, 429 (2001).
12. Z. Wang, D. Flototto, and E.J. Mittemeijer, *J. Appl. Phys.* 121, 095307 (2017).
13. H. Fujiwara, T. Kaneko, and M. Kondo, *Sol. Energy Mater. Sol. Cells* 93, 725 (2009).
14. J. Müllerová, P. Šutta, G. van Elzakker, M. Zeman, and M. Mikula, *Appl. Surf. Sci.* 254, 3690 (2008).
15. R. Madaka, V. Kanneboina, and P. Agarwal, *J. Eectron. Mater.* 47, 4710 (2018).
16. R. Madaka, V. Kanneboina, and P. Agarwal, *J. Mater. Sci. Mater. Electron.* 28, 8885 (2017).
17. A.F. i Morral, P.R. i Cabarrocas, and C. Clerc, *Phys. Rev. B* 69, 125307 (2004).
18. K. Saitoh, M. Kondo, M. Fukawa, T. Nishimiya, and A. Matsuda, *Appl. Phys. Lett.* 71, 3403 (1997).
19. H. Fujiwara, *Spectroscopic Ellipsometry: Principles and Applications* (John Wiley & Sons Ltd., 2007).
20. S. Hamma and P.R. i Cabarrocas, *Sol. Energy Mater. Sol. Cells* 69, 217 (2001).
21. L. Korte and M. Schmidt, *J. Non Cryst. Solids* 354, 2138 (2008).
22. S.A. Filonovich, M. Ribeiro, A.G. Rolo, and P. Alpuim, *Thin Solid Films* 516, 576 (2008).
23. R. Saleh and N.H. Nickel, *Sol. Energy Mater. Sol. Cells* 90, 3456 (2006).
24. A.K. Kesarwani, O.S. Panwar, R.K. Tripathi, M.K. Dalai, and S. Chockalingam, *Mater. Sci. Semicond. Process.* 31, 1 (2015).
25. A. Descoeudres, L. Barraud, S. De Wolf, B. Strahm, D. Lachenal, C. Guérin, Z.C. Holman, F. Zicarelli, B. Demaurex, J. Seif, J. Holovsky, and C. Ballif, *Appl. Phys. Lett.* 99, 123506 (2011).
26. S. De Wolf, A. Descoeudres, Z.C. Holman, and C. Ballif, *Green* 2, 7 (2012).

27. V. Kanneboina, R. Madaka, and P. Agarwal, *Mater. Today Commun.* 15, 18 (2018).
28. V. Kanneboina, R. Madaka, and P. Agarwal, *Sol. Energy* 166, 255 (2018).
29. G.E. Jellison and F.A. Modine, *Appl. Phys. Lett.* 69, 371 (1996).
30. D.A.G. Bruggeman, *Ann. Phys.* 416, 636 (1935).
31. D.E. Aspnes, *Thin Solid Films* 89, 249 (1982).
32. T. Yuguchi, Y. Kanie, N. Matsuki, and H. Fujiwara, *J. Appl. Phys.* 111, 083509 (2012).
33. L.R. Dahal, J. Li, J.A. Stoke, Z. Huang, A. Shan, A.S. Ferlauto, C.R. Wronski, R.W. Collins, and N.J. Podraza, *Sol. Energy Mater. Sol. Cells* 129, 32 (2014).
34. R.W. Collins, A.S. Ferlauto, G.M. Ferreira, C. Chen, J. Koh, R.J. Koval, Y. Lee, J.M. Pearce, and C.R. Wronski, *Sol. Energy Mater. Sol. Cells* 78, 143 (2003).
35. S. Kageyama, M. Akagawa, and H. Fujiwara, *Phys. Rev. B* 83, 195205 (2011).
36. H. Zhang, X. Zhang, G. Hou, C. Wei, J. Sun, X. Geng, S. Xiong, and Y. Zhao, *Thin Solid Films* 521, 17 (2012).
37. Y.-H. Chu, C.-C. Lee, I.-C. Chen, S.-Y. Chang, J.-Y. Chang, and T. Li, *Thin Solid Films* 570, 591 (2014).
38. A.F. i Morral and P.R. i Cabarrocas, *J. Non Cryst. Solids* 299–302, 196 (2002).
39. W. Beyer, *Sol. Energy Mater. Sol. Cells* 78, 235 (2003).
40. J. Tauc, R. Grigorovici, and A. Vancu, *Phys. Status Solidi* 15, 627 (1966).
41. P. Gogoi, H.S. Jha, and P. Agarwal, *J. Non Cryst. Solids* 358, 1990 (2012).
42. Z. Remes, M. Vanecek, P. Torres, U. Kroll, A.H. Mahan, and R.S. Crandall, *J. Non Cryst. Solids* 227–230, 876 (1998).